Alignment validation

Tobias Golling

This work was supported by the Director, Office of Science, Office of Basic Energy Sciences, of the U.S. Department of Energy under Contract No. DE-AC02-05CH11231.

Alignment validation

T. Golling[a]
for the ALICE, ATLAS, CMS and LHCb Collaborations

[a] *Lawrence Berkeley National Laboratory*
Berkeley, USA

Abstract
The four experiments, ALICE, ATLAS, CMS and LHCb are currently under construction at CERN. They will study the products of proton-proton collisions at the Large Hadron Collider. All experiments are equipped with sophisticated tracking systems, unprecedented in size and complexity. Full exploitation of both the inner detector and the muon system requires an accurate alignment of all detector elements. Alignment information is deduced from dedicated hardware alignment systems and the reconstruction of charged particles. However, the system is degenerate which means the data is insufficient to constrain all alignment degrees of freedom, so the techniques are prone to converging on wrong geometries. This deficiency necessitates validation and monitoring of the alignment. An exhaustive discussion of means to validate is subject to this document, including examples and plans from all four LHC experiments, as well as other high energy experiments.

11.1 Motivation for validation

Track-based alignment algorithms [1–3] have an intrinsic problem: They use a one-dimensional quantity, the track residual, to extract six or more degrees of freedom per module, where a module refers to the smallest detector element to be aligned. The degrees of freedom consist of three translations, three rotations and possibly a few additional parameters describing typical deformations of the module. Thus, it is not unlikely that the algorithms converge but the predicted positions of the modules do not correspond to the real ones. Hardware-based alignment procedures have similar shortcomings.

As a consequence a thorough validation and if necessary a correction of the alignment is required. Obviously, all kinds of misalignments which alter the reconstruction of the underlying physics need to be eliminated. An alignment validation guideline can be yielded by inverting this argument: If the physics observables are unchanged by a certain misalignment then it does not need to be removed, e.g., a global rotation of the whole detector.

The validation is based on diverse additional information that is used to impose constraints, e.g., track data sets with different topologies or different run conditions, known physics properties, low level distributions, or external constraints. If possible the alignment validation should feed back into the alignment algorithms as implementations of additional constraints, otherwise it should serve as an alignment monitoring tool. This monitoring tool can also be used to monitor tracking or reconstruction in general. The goal of the alignment and its validation can be subdivided in three phases.

- Beginning of data taking: provide an alignment which does not break the tracking reconstruction, make sure that the alignment can not be used as a scapegoat.
- As the data increases: take full advantage of increased statistics, control systematics.
- Ultimately: provide the best alignment possible.

The alignment validation is in principle very similar for all four experiments. The general, experiment-independent ideas will be presented using examples from LHC and non-LHC experiments. At the end differences between the LHC experiments will be pointed out.

A discussion of typical misalignment scenarios is presented in Section 11.2. Section 11.3 focuses on specific techniques to control individual misalignments. More general approaches to make the alignment algorithms more robust, by using different track data sets, are presented in Section 11.4. Methods to disentangle energy loss, magnetic field and alignment effects are discussed in Section 11.5. An important part of the

alignment validation makes use of Monte Carlo simulation as shown in Section 11.6. If all else fails residual misalignments can be caught by a detailed alignment monitoring, see Section 11.7. A summary and conclusion is given in Section 11.8.

If not stated otherwise, coordinates refer to the global coordinate system of the detector, where the z-axis is parallel to the beam axis.

11.2 Categorization of systematic misalignments

It was mentioned earlier that the system of degrees of freedom for the detector alignment is under-constrained. More specifically this means there are classes of detector distortions, also referred to as 'weakly determined modes', i.e., misalignments, that alter the shape of tracks in such a way that they remain helical, or almost helical, but with certain track parameters modified and systematically biased. It is useful to introduce a few definitions that facilitate the discussion of the various misalignments:

Level 1 misalignment refers to the position and orientation of whole subdetectors with respect to each other.

Level 2 misalignment refers to a misalignment of whole layers, cylinders for the barrel part and discs for the end-caps.

Level 3 misalignment refers to misalignments of individual modules.

It is expected that the initial misalignments are largest on level 1 and smallest on level 3 due to construction precision and installation circumstances.

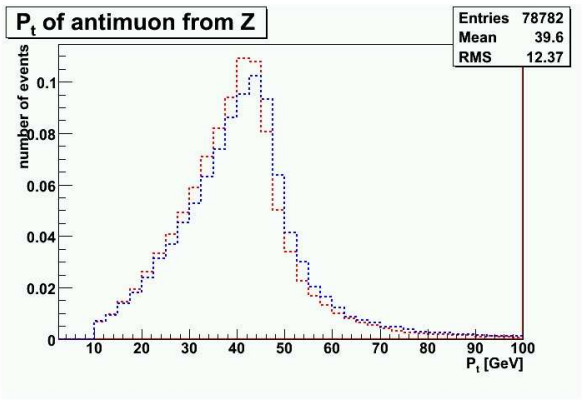

Fig. 11.1: Transverse momentum distribution of positively and negatively charged muons from Z decays in presence of an $r\phi$ sagitta distortion, reconstructed in the CMS detector [4]

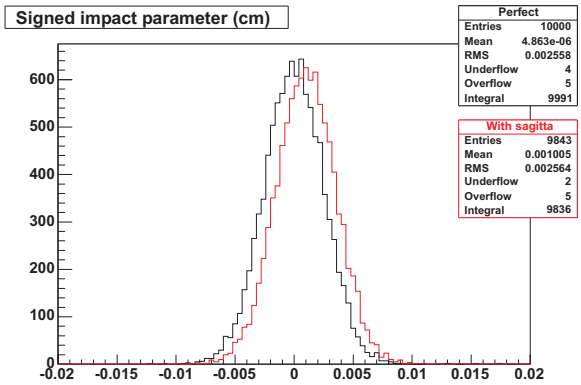

Fig. 11.2: Signed transverse impact parameter for muons with a p_{t} of 40 GeV with and without an $r\phi$ sagitta distortion with a non-zero 'constant term' c, reconstructed in the ATLAS detector [5]

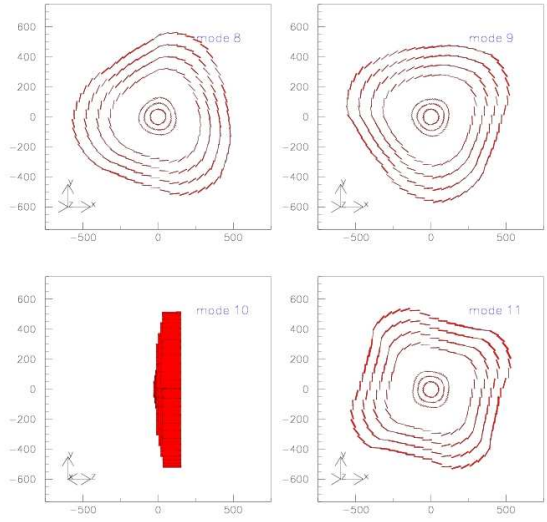

Fig. 11.3: Some examples of lowest frequency modes, which approximately transform track helices into other helices, for the ATLAS Pixel and SCT barrel [3]: Mode 8, 9 and 11 show projections of the modules in the three Pixel and four SCT barrels onto the x-y-plane. Mode 10 shows the 'telescoping' effect in a projection of all modules in a ring for all seven barrel layers onto the y-z-plane.

11.2.1 Misalignment of whole subdetectors

A relative translation or rotation of two subdetectors can be identified by reconstructing tracks separately and interpolating them onto a common surface somewhere in the middle, where the five track parameters can be compared. Alternatively the relative alignment of two sub-

detectors can be deduced from the separate reconstruction of the beamline, as done by CDF for the COT and the SVX [6]. A decision needs to be taken which of the subdetectors should be kept fixed.

11.2.2 Sagitta distortions

Here sagitta distortions refer to level 2 misalignments which transform helical into helical tracks, but systematically bias the track parameters. Typically, the alignment algorithms converge on sagitta distortions of the same size as the initial random misalignments of the layers. This is true for all degrees of freedom and is exemplified in the following for barrel layers and in the high transverse momentum (p_{t}) limit where tracks become parabolic [5]:

$r\phi$ **rotations (rotations about the z-axis):** Layers are left progressively rotated about the z-axis according to

$$\Delta r\phi \propto ar^2 + br + c, \qquad (11.1)$$

where r = radius. The 'quadratic term' a in Eq. (11.1) introduces a p_{t} bias, opposite for positively and negatively charged particles, as shown in Fig. 11.1. The 'linear term' b causes a global rotation of all barrels by the same angle and the 'constant term' c introduces a bias on the transverse impact parameter (d_0), as shown in Fig. 11.2.

z **translations:** Layers are left progressively translated in the z-direction proportional to $dr + e$, referred to as 'telescoping' and visualized in the bottom left of Fig. 11.3. The longitudinal impact parameter and the η of the track are biased.

x/y **translations:** Layers are left progressively translated in the x/y-direction, as shown on the top left of Fig. 11.4.

x/y **rotations (rotations about the x/y-axes):** Layers are left progressively rotated about the x/y-axes.

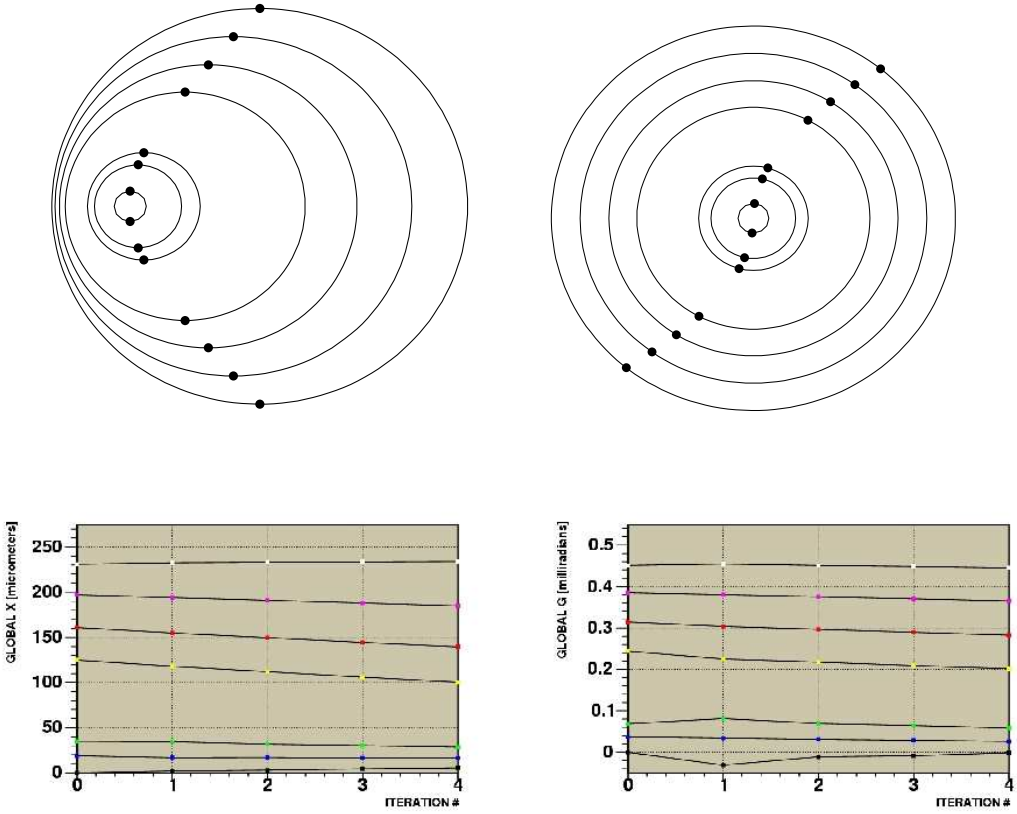

Fig. 11.4: Top: Visualization of sagitta distortions for the three Pixel barrel layers (inner) and the four SCT barrel layers (outer) of the ATLAS detector [5]. Bottom: Initial misalignment as shown in the corresponding top sketches and residual misalignments after the first four alignment iterations of all barrel layers, using the algorithm in [2]. The misalignment grows from inside out, i.e., from the inner Pixel to the outer SCT layer of the ATLAS detector [7]. Left: translation in x. Right: $r\phi$ rotation.

Figure 11.4 demonstrates the insensitivity of track-based alignment algorithms to these sagitta distortions, exemplified for a translation in x (left) and a non-zero 'quadratic term' a, see Eq. (11.1), of an $r\phi$ rotation (right). The distortions do not impact the track reconstruction, they only alter the parameters, i.e., p_{t}, direction and impact parameter, of the track helix fit. As a consequence it is impossible for the alignment algorithms to recover the distortions.

11.2.3 More generic high-frequency modes

The systematic distortions described in Section 11.2.2 involve only level 2 misalignments. They are part of a whole spectrum of level 3 misalignments, i.e., systematic translations and rotations of modules which approximate systematic deformations of layers, see Fig. 11.3. These misalignments again can lead to significant biases in the reconstructed track parameters, as discussed in Section 11.2.2. However, they are expected to have a smaller amplitude given the smaller initial misalignments at level 3 (as compared to level 2).

These misalignment modes can be identified with the low part of the eigenspectrum of orthogonal mode solutions to the Global χ^2 alignment problem. 'Global' refers to the fact that the χ^2 is minimized with respect to all alignment and track degrees of freedom simultaneously retaining all actual correlations. The eigenspectrum for the ATLAS silicon tracking system is shown in Fig. 11.5.

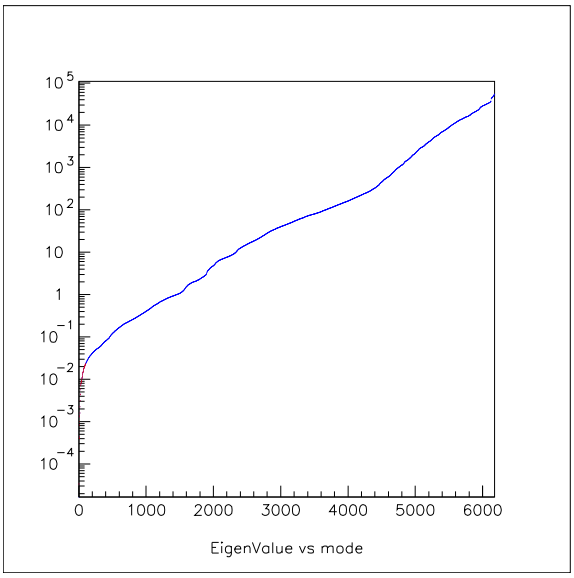

Fig. 11.5: Eigenvalue spectrum of the orthogonal mode solutions to the Global χ^2 algorithm described in [3]. Total number of modes is equal to the number of all alignment parameters. The uncertainty on the alignment parameter is given by the square root of the reciprocal of the eigenvalue. Consequently, the lowest modes dominate the overall error on the alignment.

11.3 Methods to control weakly determined modes

Sagitta distortions, as described in Section 11.2 persist even if the underlying track set consists of tracks at different momenta and different sign charge. However, there are other handles which can help to control the distortions.

11.3.1 Magnetic field off

If no magnetic field were present in the inner detector, the alignment procedure would be unable to converge on a p_{t}-biasing sagitta distortion since the tracks would be forced to be of infinite momentum, i.e., straight tracks. The drawback is that the presence of the magnetic field itself introduces a misalignment and a shift of the reconstructed hit according to the Lorentz shift. A minor point is the fact that without magnetic field no transverse momentum measurement is possible, which is needed for the multiple scattering estimation.

ALICE and LHCb plan to do the main alignment with data taken without magnetic field. The field is relatively small, 0.5 T, as compared to 2 and 4 T for ATLAS and CMS, and in contrast to ATLAS and CMS, ALICE and LHCb will reverse the polarity of the magnetic field during data taking.

11.3.2 Redundancy of the whole detector

Position, energy and momentum of a charged particle are usually measured by more than one subsystem. This redundancy can be used to impose additional constraints on the alignment algorithms.

11.3.2.1 Redundant momentum measurements

Direct constraints on track parameters are a good means to control biases. Momentum information can be used from either the muon system or an already aligned tracking subsystem.

11.3.2.2 Redundant position measurements

The electromagnetic calorimeter provides precise position measurements that can be compared with extrapolated track positions, as done in Ref. [8]. The ATLAS electromagnetic Liquid Argon calorimeter has a position resolution of approximately 1 mm. Studies have shown that 10k $Z \rightarrow e^+e^-$ events are sufficient to reach an alignment sensitivity much better than 1 mm for translations and 1 mrad for rotations, and it is possible to detect sagging effects of the inner detector [8].

Figure 11.6 shows an example of a relative calorimeter-tracker translation.

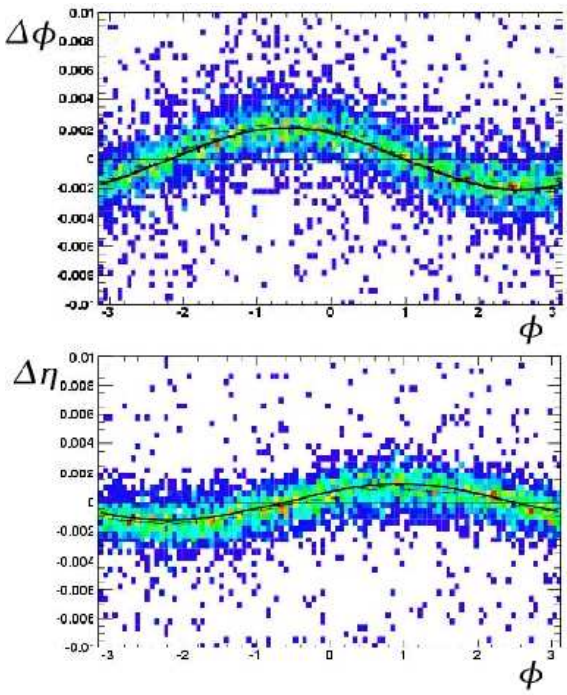

Fig. 11.6: $\Delta\phi$ (top) and $\Delta\eta$ (bottom) of reconstructed calorimeter clusters and extrapolated track positions *vs.* ϕ for 10k $Z \rightarrow e^+e^-$ events for a relative calorimeter-tracker translation of 2 mm in x and 3 mm in y [8]

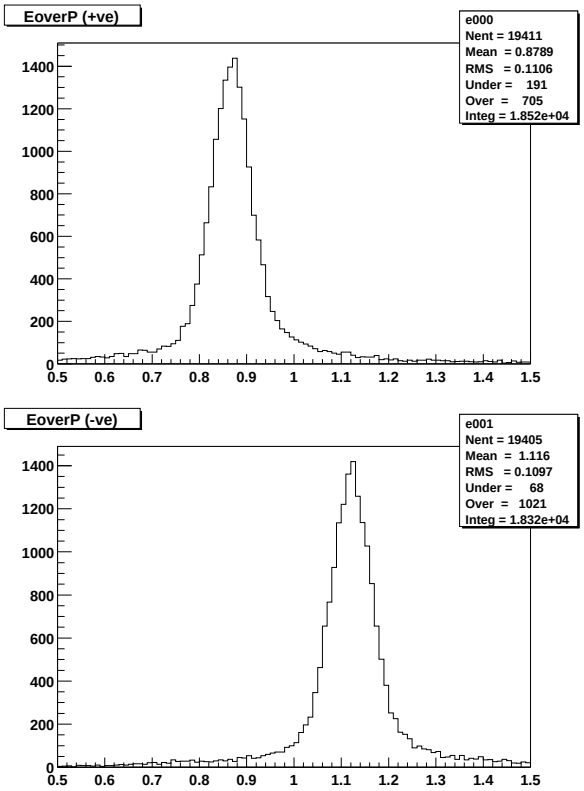

Fig. 11.7: E/p for positrons (top) and electrons (bottom) with a p_{t} of 40 GeV in the ATLAS detector for an $r\phi$ sagitta distortion with a non-zero 'quadratic term' a, as given in Eq. (11.1) and shown in the top right of Fig. 11.4 [5]

11.3.2.3 Energy–momentum relation

The energy of an electron can be measured very precisely in the calorimeter. The ratio of energy over momentum (E/p) of a charged particle is centred approximately at the value of one, with tails, caused by bremsstrahlung. The E/p ratio plotted separately for positively ($+$) and negatively ($-$) charged particles is biased away from one in opposite directions, in presence of a non-zero 'quadratic term' a of an $r\phi$ sagitta distortion (Eq. (11.1)), see Fig. 11.7. The distortion can be deduced from these distributions by e.g., using the E/p peak positions:

$$\Delta\frac{1}{p} = \frac{E/p_+ + E/p_-}{E_+ + E_-}. \qquad (11.2)$$

The sagitta distortion is proportional to $\Delta\frac{1}{p}$.

At the beginning of data taking the calorimeter calibration will not be available. A crucial feature of this measurement is that the calorimeter calibration is not necessary. It is only required that E/p be independent of the particle's charge, which is given, neglecting the level of a few MeV.

11.3.3 Known symmetries

Charge, forward–backward or ϕ-symmetries of physics processes can be used to probe the presence of weakly determined modes. In principle the 'telescoping' effect creates a forward–backward asymmetry. However, the sensitivity is very low. The nominal signed impact parameter distribution has a mean of zero. An $r\phi$ sagitta distortion with a non-zero 'constant term' c of Eq. (11.1) introduces a shift in this distribution, see Fig. 11.2. This shift is ϕ-dependent if the track origin is not determined properly.

11.3.3.1 Charge dependence

$\Delta\frac{1}{p}$ can be directly extracted from a distribution of tracks which is known to be charge symmetric, as is the case for the process $Z \rightarrow \mu^+\mu^-$. In the presence of an $r\phi$ sagitta distortion the p_{t} distributions for positively and negatively charged muons are shifted in opposite directions, see Fig. 11.1. The Z mass itself, however, is hardly affected by this misalignment since the momentum biases cancel approximately in the mass determination: $M_Z^2 = 2p_1p_2(1-\cos\theta_{12})$.

11.3.4 Beam spot, vertex constraint

A beam spot or vertex constraint can remove the 'constant term' c of Eq. (11.1), the part of the $r\phi$ sagitta distortion, which results in a transverse impact parameter bias. The constraint leads to an improved sensitivity to the low modes discussed in Section 11.2.3 and reduced errors on the module positions, in particular close to the interaction point, see Fig. 11.8.

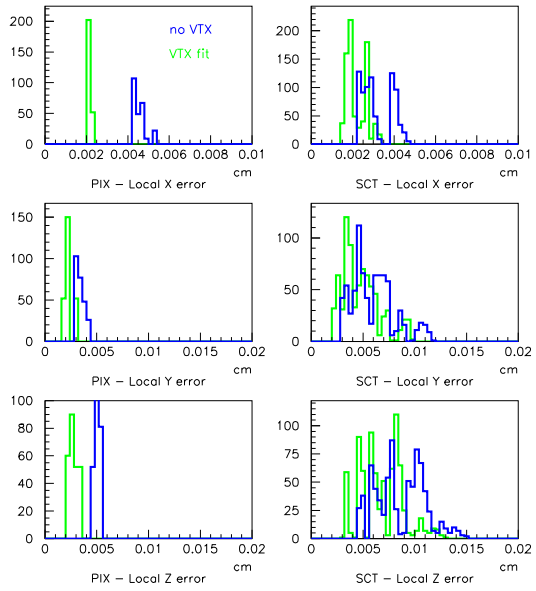

Fig. 11.8: Errors on the Pixel (left) and SCT (right) positions of the ATLAS detector, using the algorithm in [3] with (light) and without (dark) vertex fit, using 450k muon tracks with p_{t} between 2 and 20 GeV

11.3.5 Overlap hits

Modern silicon tracking detectors are built of several layers of silicon around the interaction region. Layers are built of overlapping modules to avoid holes in the detector. Tracks traversing these overlap regions can be used to study the relative positions of adjacent modules by creating a new type of hit residual called an 'overlap residual'. This 'overlap residual' is defined as the difference of the two hit residuals in the outer and the inner module. Module overlaps typically exist in z and $r\phi$ [5, 9].

Whereas regular hit residuals allow one to align modules in different layers, the 'overlap residuals' add new information on the relative position and orientation of adjacent modules in the same layer, and they uniquely allow one to impose a circumference constraint. However, usually only a small fraction of tracks pass through the overlap regions.

Errors on the residuals in two overlapping layers are highly correlated and can be subtracted out. This is particularly true for uncertainties arising from multiple scattering since the track extrapolation error is so much smaller, given the proximity of the overlapping layers. This fact also allows one to utilize tracks with lower transverse momentum. Overlap residuals are very robust and only marginally affected by misalignments elsewhere in the detector. More precisely, the overlap residual equals the size of the relative misalignment between the overlapping modules as long as the angle of incidence of the track is unaltered.

11.3.6 External constraints

Relative positions and orientations of detector elements are precisely measured before the final installation. This survey data is particularly useful to constrain neighbouring modules on rigid structures. For overlapping modules cross-checks with the method discussed in Section 11.3.5 can be performed. A lot of survey data is subject to change in the process of installation and needs to be discarded from alignment applications. A method to incorporate survey data in alignment algorithms is explained in Ref. [10]. Similar information can be deduced from hardware alignment systems.

The muon spectrometers are expected to move up to a few millimetres during the installation of the whole detector. As a consequence survey data taken prior to the installation is not very useful for alignment purposes. Optical hardware alignment systems are used instead to measure relative positions and orientations of detector elements *in situ*. Usually, not all degrees of freedom can be constrained and a combination with track-based alignment information is essential.

11.4 Track data sets with different topologies

Another means to control weakly determined modes is to include many different data sets in the track-based alignment algorithms used. Dominantly, tracks from proton–proton collisions are used for this purpose. The advantage of this sample is its large statistics, given the luminosity, and the large variety of processes, given the production cross-section. The problem, however, is that all tracks originate from the beam spot and as a consequence tracks hitting a certain module traverse only a small number of other modules, in the worst case only one module per layer. It is therefore useful to add tracks which traverse different sets of modules given by data sets with different track origins.

In general, the pattern recognition needs to be modified to find tracks with origins different from the nominal interaction point. Monte Carlo simulations can be used to study pattern recognition and the possibilities to trigger on these events.

11.4.1 Cosmic muons

Before the start-up of the LHC machine it will be possible to operate the detector and to record cosmic events. Cosmic muons are the only tracks that link the top to the bottom hemisphere of the tracking detector. This unique property makes them very valuable, in particular to constrain the 'telescoping' effect. The cosmic rate decreases strongly as the incident angle deflects from the vertical. The cosmic particle spectrum is very soft. The depths of the detectors further decreases the rate of tracks usable for alignment.

It is very desirable to take cosmic events as well during collision data, given the unique properties of cosmic muon tracks. This can be done either in special runs in-between colliding beam operation or continuously with dedicated cosmic triggers during the actual proton–proton collisions.

Even before the various tracking subdetectors are installed in their final position in the experiment they can be exposed to cosmic rays. This has been done for all four LHC experiments and has proven very useful to exercise the whole alignment effort.

11.4.2 Single beam

Before the first proton–proton physics collisions there will be a single beam operation. One can try to use tracks for alignment which are considered background in the colliding beam operation:

Halo muons Halo muons originate from beam halo protons which collide with the beam apertures, e.g., a collimator, and produce a shower of secondary halo particles which eventually decay to halo muons. These muons are mainly parallel to the beam line but can have distances of a few metres in the transverse direction and can reach momenta close to the initial beam energy [11]. Halo muons are the only tracks that link the forward to the backward region. A relative alignment of disks within an end-cap and of the two end-caps with respect to each other is possible.

Beam-gas Beam-gas interactions are collisions of protons from the beam with the residual gas. The rate depends on the vacuum conditions and the rest gas composition. The vacuum is usually good around the interaction point and bad around the outgassing collimators. The events are characterized by a small centre-of-mass energy (28 GeV for 450 GeV beam energy and 113 GeV for 7 TeV beam energy, treating the gas atoms as fixed targets), low momentum tracks and tracks in the very forward [11].

11.4.3 900 GeV run and parasitic collisions

The first LHC colliding run at the end of 2007 will be at a centre-of-mass energy of 0.9 TeV instead of 14 TeV. At 0.9 TeV head-on collisions at LHCb require collisions displaced in z, so-called 'parasitic collisions', at the other three experiments, and vice versa. These parasitic collisions occur for two reasons:

- The LHCb detector is displaced from the LHC symmetry point due to its asymmetric shape.
- At 0.9 TeV the beams will have no crossing angle in contrast to the 14 TeV run.

The parasitic collisions can be tuned to occur between 37.5 cm and several metres away from the nominal interaction point in z. These parasitic events occur at a much lower rate, O(10%), and the luminosity ratio decreases as one goes away from the nominal interaction point (estimates give 50% for 11 m and 90% for 4 m) [12]. Interactions which are too far from the centre of the detector will not illuminate the tracking system. Studies are ongoing both at ATLAS and CMS to estimate the alignment benefits of these data sets.

Another benefit of the 900 GeV run is the possibility to trigger on J/Ψ's and Υ's decaying to muons, which is very challenging at 14 TeV [13]. This allows to use the method discussed in Section 11.3.3.1, as well as the disentanglement of alignment and other effects, see Section 11.5.

11.4.4 Combination of data sets

The best performance of the alignment algorithm is given by combining all the various data sets according to their sensitivity to misalignments, including overlap hits from Section 11.3.5 and hits from tracks which traverse both the barrel and the end-cap. This can be done either by using weights or prescale factors. The latter is easier to implement. A prescale factor on hit level (as compared to track level) has the advantage of reducing statistical correlations, which are introduced since the track information is used multiple times, for each module it traverses.

Prescaling in transverse momentum, pseudorapidity and vertex z position leads to further sensitivity improvements and to a more uniform illumination of the detector components.

11.5 Disentanglement of energy loss, magnetic field and alignment

It is crucial to disentangle misalignment effects from other sources of systematic biases. Both an inadequate description of the material budget and of the magnetic field can result in very similar biases in the track parameters. Their disentanglement makes use of the invariant mass of J/Ψ's and Υ's decaying to muon pairs.

At low p_t the mass is very sensitive to the energy loss of charged particles, and therefore the material budget. Magnetic field effects are independent of the particle's charge whereas alignment effects are not. The method is usually iterative and includes the use of photon conversions and K_s's [14].

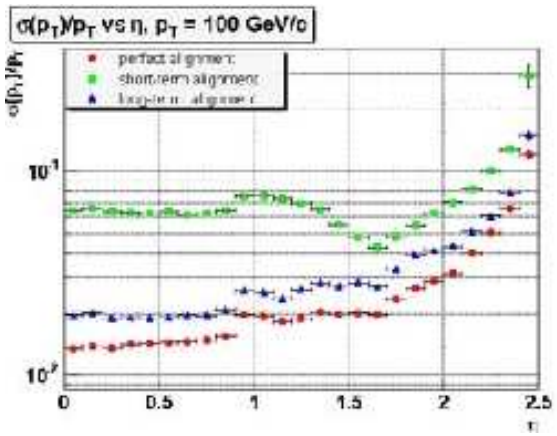

Fig. 11.9: Impact of misalignment on the transverse momentum resolution as a function of η for single muons in CMS [15]

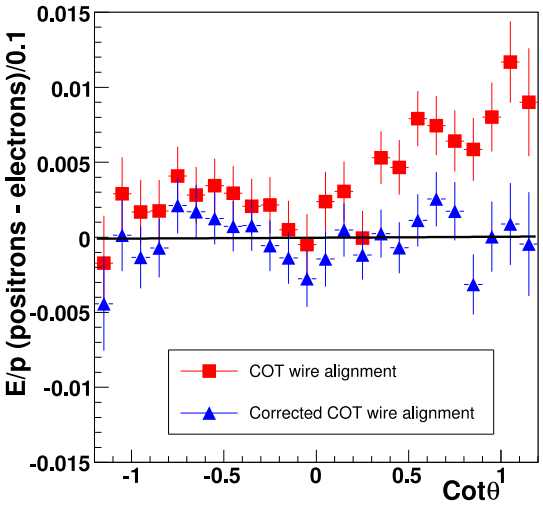

Fig. 11.10: Difference in E/p for positrons and electrons before and after a curvature correction applied to the alignment in CDF [16]

11.6 Alignment validation with Monte Carlo simulation

Track-based alignment algorithms can be tested for their robustness against misalignments before real data becomes available using Monte Carlo simulation. In particular the improvements that are discussed in Sections 11.3 and 11.4 can be verified.

There are two different ways of implementing misalignments in the Monte Carlo simulation: either at the simulation level, by physically moving the detector elements in GEANT, or at the reconstruction level, by moving the reconstructed hits in the opposite direction. Inserting misalignments at the two stages is roughly equivalent with the following exceptions.

- Implementing misalignments at the simulation level is much more time consuming. A change in the misalignment requires re-simulation.
- Tracks are never caused to miss misaligned modules if misalignments are implemented at the reconstruction level as may be the case for misalignments at the simulation level.
- At the reconstruction level hits can be moved before or after the pattern recognition which impacts the track reconstruction efficiency.

Apart from these differences the alignment results are very similar for the two misalignment implementations [17]. This allows to do many alignment robustness studies with misalignments inserted at the reconstruction level.

An arbitrary misalignment can be described as a combination of 'typical misalignments', or a 'basis of misalignments', as discussed in Section 11.2. While it is impossible to construct all possible misalignments it can be aspired to built a few typical and realistic misalignments, a 'matrix of misalignments', which populate the characteristic regions of the 'misalignment phase space'.

Application of the alignment algorithms to this 'matrix' shows to what extent misalignments can be recovered and it gives an estimate of the expected systematic uncertainties. However, only the data can tell, so one has to stay alert and prepare for surprises, as discussed in Section 11.7.

11.7 Alignment monitoring

Even after the validation of the alignment as discussed in the previous sections it is not guaranteed that the alignment is free of systematic effects. The best preparation for 'the unexpected' is a detailed monitoring tool which checks for consistency of the data. In addition the alignment is expected to change with time. The monitoring can be used to assess the need for a reevaluation of alignment constants.

BaBar [18] validates, and updates if necessary, its alignment every two weeks using monitoring. Roughly 40 alignment periods are identified, separated by detector interventions or humidity effects.

Here are just a few examples of distributions which have sensitivity to residual misalignments:

- The momentum resolution of charged particles is a good indicator of detector misalignments, as shown in Fig. 11.9. The mass resolution of e.g., J/Ψ's, Υ's, Z's or other hadrons is a good measure of the momentum resolution and can be used alternatively.
- $\Delta\frac{1}{p}$ as given in Eq. (11.2) is a good quantity to plot as a function of track parameters. CDF used it to derive and validate curvature corrections [16], see Fig. 11.10.
- $\Delta\phi$ and $\Delta\eta$ of reconstructed tracks and the corresponding electromagnetic clusters *vs.* ϕ or *vs.* z.
- Track parameters as a function of other track parameters, e.g., transverse and longitudinal impact parameter *vs.* ϕ or η.
- Mean and σ of $r\phi$ position of primary vertex *vs.* z.
- Track residual distributions *vs.* the position in the module. Patterns can give information about module deformations.

11.8 Summary and conclusion

The alignment task for the four LHC experiments, with a number of alignment degrees of freedom up to 100k for CMS, is highly non-trivial. The alignment result cannot be trusted without a thorough validation. The validation techniques are manifold and are summarized here.

- Tracks recorded without the presence of a magnetic field impose different constraints and can be used to deduce or cross-check alignment information.
- Modern particle detectors such as the LHC experiments provide many redundant energy, momentum and position measurements, which can be exploited for alignment validation.
- Alignment shortcomings can be identified if they alter characteristic symmetries and properties of the underlying physics, such as charge, forward–backward or ϕ-symmetries.
- Overlap residuals provide additional orthogonal alignment information to the conventional hit residuals.
- External constraints and hardware alignment techniques complement track-based alignment methods.
- Track data sets with different topologies represent an invaluable tool for alignment validation. Most notably cosmic events, representing off-axis tracks across the whole detector volume, but also halo muons, beam-gas events or parasitic collisions.
- Monte Carlo simulation allows to test the alignment algorithms as well as the alignment validation process.
- A detailed alignment monitoring represents the last instance of alignment validation, which hopefully catches also 'the unexpected' alignment peculiarities.

Many alignment validation handles can be converted to alignment constraints, which can be imposed during the alignment process itself, as shown in Ref. [10].

The alignment and its validation is very similar for ATLAS and CMS. Both inner detector systems have large magnetic fields and are composed of a lot of material which necessitates the use of high p_{t} tracks. No magnet-off data is planned to be used. ALICE and LHCb, however, have very little material and relatively small magnetic fields. Alignment will be done mainly with magnet-off data. Some peculiarities are that the ALICE detector does not have full electromagnetic coverage, so the E/p method mentioned in Section 11.3.2.3 can not be used, and LHCb has basically no acceptance for cosmic events (Section 11.4.1), since it is only interested in forward physics.

Acknowledgements

I wish to thank F. Bauer, S. Blusk, D. Brown, P. Bruckman, O. Buchmueller, R. Culbertson, R. Grosso, A. Heijboer, A. Jacholkowski, A. Korn, R. Madaras, F. Matorras, J. Nardulli, M. Scherzer, J. Schieck, F. P. Schilling, M. Stoye, S. Viret, L. Winstrom, C. Young, F. Zimmermann and the entire LHC alignment community for enlightening comments on the present topic.

References

[1] V. Karimäki *et al.*, CMS Note 2006/018 (2006); R. Frühwirth *et al.*, CMS Note 2006/022 (2006); P. Schleper *et al.*, CMS Note 2006/011 (2006).

[2] R. Härtel, Diploma thesis, Technische Universität München (2005), available at `http://publications.mppmu.mpg.de/?year=2005&action=search&author=h.rtel&researchfield=&genre=&title=&format=WWW`;
T. Göttfert, Diploma thesis, Universität Würzburg (2006), available at `http://publications.mppmu.mpg.de/?year=2006&action=search&author=g.ttfert&researchfield=&genre=&title=&format=WWW`.

[3] P. Brückman de Renstrom and S. Haywood, Proceedings of PhyStat05, L. Lyons and

M.K. Ünel (Eds.) (Imperial College Press, London, 2006).

[4] M. Stoye, private communication.

[5] D. Hindson, Ph. D. thesis, Oxford University (2004), available at http://www-pnp.physics.ox.ac.uk/~hindson/thesis.shtml.

[6] R. Culbertson and A. Heijboer, private communication.

[7] M. Scherzer, private communication.

[8] R. Zitoun, talk at the ATLAS $e\gamma$ meeting (2006), available at http://indico.cern.ch/conferenceDisplay.py?confId=a058233.

[9] F. Heinemann, DPhil. Thesis, Oxford University (2007).

[10] T. Golling, ATL-INDET-PUB-2006-001 (2006).

[11] M. Boonekamp *et al.*, ATL-GEN-2004-001 (2004).

[12] C. Young and F. Zimmermann, private communication.

[13] D. Green, private communication, see also URL http://vmsstreamer1.fnal.gov/VMS_Site_03/Lectures/HCPSS/presentations/060817Green.pdf.

[14] D. Acosta *et al.* [CDF Collaboration], *Phys. Rev. Lett.* **96** (2006) 202001 [arXiv:hep-ex/0508022].

[15] CMS Collaboration, CERN/LHCC 2006-001 (2006).

[16] A. Kotwal, Joint Experimental-Theoretical Seminar at Fermilab, available at http://theory.fnal.gov/jetp/talks/kotwal.pdf (2007).

[17] ATLAS Computing System Commissioning (CSC), wiki available at https://twiki.cern.ch/twiki/bin/view/Atlas/ComputingSystemCommissioning.

[18] D. Brown, private communication.